Investigation of the Impact of a Chemical Reaction on the Magnetohydrodynamic Boundary Layer Flow of a Radiative Maxwell Fluid over a Stretching Sheet Containing Nanoparticles Employing the Variational Iteration Method

AMINE EL HARFOUF[1,*], ABDERRAHIM WAKIF[2], SANAA HAYANI MOUNIR[1]
[1]Multidisciplinary Laboratory of Research and Innovation (LaMRI),
Energy, Materials, Atomic and Information Fusion (EMAFI) Team,
Polydisciplinary Faculty of Khouribga,
Sultan Moulay Slimane University,
MOROCCO

[2]Faculty of Sciences Aïn Chock, Laboratory of Mechanics,
Hassan II University,
Casablanca,
MOROCCO

**Corresponding Author*

Abstract: - The heat and mass transmission properties of a 2-D electrically conducting incompressible Maxwell fluid past a stretched sheet were studied under thermal radiation, heat generation/absorption, and chemical reactions. This issue has a variety of real-world applications, most notably polymer extrusion and metal thinning. The transport equations account for both Brownian motion and thermophoresis during chemical reactions. Using similarity variables allows for non-dimensionalization of the stream's PDEs and associated boundary conditions. The resulting modified ODEs are solved with the variational iteration approach. The impact of embedded thermo-physical variables on velocity, temperature, and concentration was studied quantitatively. When compared to the RK-Fehlberg approach, the findings are very similar. Raising the chemical reaction parameter narrows the concentration distribution, whereas increasing the temperature increases thermal radiation's impact. As the amount of N_t increases, the thickness of the boundary layer develops, causing the surface temperature to rise, resulting in a temperature increase.

Key-Words: - Chemical reaction, Nanoparticles, Maxwell fluid, Stretching sheet, Thermal radiation, the variational iteration approach, the RK-Fehlberg approach.

Received: January 12, 2024. Revised: July 11, 2024. Accepted: August 8, 2024. Published: September 23, 2024.

1 Introduction

Nanotechnology has enabled the creation of particles smaller than $100\,nm$. Nanoparticles are added to form a stable suspension and potentially improve the thermal characteristics of the base fluid. Adding small amounts of metal or metal oxide nanoparticles to a fluid can improve its thermal conductivity. Nanofluids, like current working fluids, may absorb and transport heat. Nanofluid flow has gained interest among researchers in various fields, including technology, science, biomechanics, chemistry, and nuclear engineering. Nanofluid technology can address technical issues such as solar energy collection, heat exchangers, and engine cooling, [1]. [2], studied the effect of Williamson nanofluid flow on an exponential stretching surface. Their findings show that the rate of heat transfer decreases with increased Brownian motion and increases with increased thermophoresis parameters. [3], studied the heat and mass transport properties of copper-aluminum oxide hybrid nanoparticles flowing over a porous medium. Their findings indicate that a porous media increase shear stresses for both pure and hybrid nanofluids. [4], propose a heat and mass transfer analysis of MHD nanofluid flow with radiative heat effects in the presence of spherical Au-metallic nanoparticles. Several scholars have studied the impact of flow-governing parameters on heat and mass transfer fluid flow problems

involving nanoparticles in various models, [5], [6], [7].

It is widely used in industrial operations such as aerodynamics, metal spinning, plastic extrusion, and condensation. The study of hydromagnetic flow past a stretching sheet has received a great deal of attention. [8], explored MHD 3-D heat and mass transfer across a stretching sheet using a water-based alumina nanofluid. They found that increasing the nanoparticle volume fraction parameter enhances heat transfer rate. [9], simulated boundary-layer flow using a nonlinear curved stretching sheet and convective mass conditions. Recent research in this area has yielded mixed results, [10], [11].

Non-Newtonian fluids' boundary layer flows have received significant interest due to their increasing use in engineering. The only way to completely understand non-Newtonian fluids and their applications is to study their flow. Engineers, physicists, and mathematicians face particular challenges when dealing with non-Newtonian fluids. Nonlinearity can manifest in diverse industries, including food, drilling, and biotechnology. Multiple models have been developed to characterize non-Newtonian fluids due to their diverse nature, making it hard to use a uniform stress-strain rate relationship. The Maxwell model describes the simplest subclass of rate-type fluids. Fluid rheology offers an alternative to Newtonian fluids. The Maxwell fluid model simplifies the physics of diluted polymeric liquids. The papers [12], [13], [14] provide instances of several approaches to addressing Maxwell fluid flows.

Thermal radiation plays a significant role in developing novel energy conversion technologies for extreme temperatures. Thermal radiation can significantly impact heat transfer in the polymer processing industry, where the quality of the end product is heavily influenced by heat management variables. Thermal radiation has a greater impact when the surface temperature differs significantly from the surrounding environment. [15], studied the thermal energy and mass transport of thinning fluids with varying shear rate viscosity. [16], investigated the effects of radiation, velocity, and thermal slippage on MHD boundary layer flow in Williamson nanofluid with porous media. Our selection of research on heat radiation's impact on MHD boundary layer movement, [17], [18], [19] has been thoroughly reviewed by scholars and analysts.

Differential equations are commonly used to explain many mechanical issues, thus the method used to solve them has a significant impact in different circumstances. Analytical solutions to low-order and simple differential equations are easy to find; however, analytical solutions to high-order or complex differential equations are difficult to obtain or may not even exist. Numerical techniques are so commonly used in practice to obtain useful findings, particularly in engineering. Ordinary differential equations (ODEs) are equations with only one independent variable that can be classified into two forms based on their boundary conditions: initial value problems (IVPs) and boundary value problems (BVPs). BVPs are more difficult to solve than other types of problems because their boundary conditions are defined at multiple points. The gunshot technique, Galerkin method, finite difference approach, finite element method, and others are popular numerical solutions for BVPs. These approaches are all capable of solving ODEs, but each has significant disadvantages. The shooting approach entails repeatedly solving the BVP's estimated IVP, which can be time-consuming for complex situations. The Galerkin technique necessitates determining a sequence of trial functions that are compatible with the boundary conditions, which are not always straightforward to calculate. In the finite difference and finite element methods, the correctness of the solution is strongly dependent on the mesh density or quality. Furthermore, all of these approaches are approximate, even those for linear ODEs.

Variational iteration method is a relatively recent approach for solving differential equations that are theoretically accurate, uses basic concepts, and converges quickly. It is based on the generic Lagrange multiplier approach for solving nonlinear equations in quantum physics, which [20], [21], [22] and [23] adapted into the variational iteration method (VIM). The VIM is essentially a generalized version of the Newton-Raphson iteration method. Furthermore, [24] recently demonstrated that when the largest derivative component is treated as the linear part in the VIM while solving nonlinear differential equations, the VIM is comparable to the well-known classical sequential approximation approach. The VIM is an excellent tool for solving differential equations, massive linear systems, and so on. It has been used to solve numerous differential equations in diverse disciplines, such as Boltzmann equation [25] in statistical mechanics.

The heat and mass transport features of an incompressible steady $2-D$ Maxwell fluid were investigated as it flowed across a stretched sheet in the presence of thermal radiation and chemical

interaction with nanoparticles. The study of hydromagnetic flow and heat transfer over a stretching sheet has received a lot of attention because of its practical applications and major impact on a variety of manufacturing processes, including aerodynamics, plastic sheet extrusion, condensation processes, and metal spinning.

The variational iteration method is used to find solutions that are similar to those that already exist and to solve reduced ODEs. When compared to the RK-Fehlberg approach, the findings are very similar.

2 Problem Description and Mathematical Formulation

In this study, we investigate a non-Newtonian Maxwell nanofluid flowing over a stretched surface that coincides with the plane $y = 0$, with a stable and laminar boundary layer. The circulation is limited to the region $y > 0$, as shown in Figure 1, where y is the coordinate measured perpendicular to the stretched surface. Furthermore, convection from a hot fluid with a temperature of T_f is thought to heat the stretching plate's bottom surface, producing a heat transfer coefficient of h_f. First order homogeneous chemical reaction processes involving species have been considered throughout this study. As the plate is stretched along the $x-axis$, the linear velocity $u_w = ax$ where "a" is a positive constant applied to it. An applied magnetic field with a constant B_0 strength is placed parallel to the flow direction along the $y-axis$. The magnetic Reynolds number is thought to be low. As a result, the induced magnetic field is not as strong as the magnetic field that is provided from outside.

The studied transport phenomena are quantified by Wakif's-Buongiorno formulation as follows, [26], [27], [28], [29], [30]:

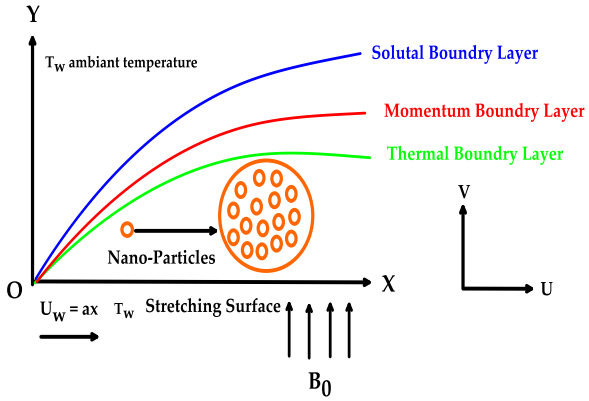

Fig. 1: Physical configuration of the model

$$\frac{\partial u}{\partial x}+\frac{\partial v}{\partial y}=0 \quad (1)$$

$$u\frac{\partial u}{\partial x}+v\frac{\partial u}{\partial y}+k_0\left(u\frac{\partial^2 u}{\partial x^2}+2uv\frac{\partial^2 u}{\partial x\partial y}+v^2\frac{\partial^2 u}{\partial y^2}\right)=+\nu\frac{\partial^2 u}{\partial y^2}-\frac{\sigma {B_0}^2}{\rho_f}\lambda\left(u+k_0 v\frac{\partial u}{\partial y}\right) \quad (2)$$

$$u\frac{\partial T}{\partial x}+v\frac{\partial T}{\partial y}=\alpha\frac{\partial^2 T}{\partial y^2}+\tau\left[\frac{D_B}{\delta_W}\frac{\partial C}{\partial y}\frac{\partial T}{\partial y}+\frac{D_T}{T_\infty}\left(\frac{\partial T}{\partial y}\right)^2\right]+\frac{Q_0}{\rho_f c_p}(T-T_\infty)-\frac{1}{\rho_f c_p}\frac{\partial q_r}{\partial y} \quad (3)$$

$$u\frac{\partial C}{\partial x}+v\frac{\partial C}{\partial y}=D_B\frac{\partial^2 C}{\partial y^2}+\frac{\delta_W D_T}{T_\infty}\frac{\partial^2 T}{\partial y^2}-k_1(C-C_h) \quad (4)$$

According to the boundary conditions:

$$u=u_w(x)=ax\,,\ v=0\,, \quad -k\frac{\partial T}{\partial x}=h_f\left(T_f-T\right)\,,\ C=C_w\,,\ \text{at } y=0 \quad (5)$$

$$u=0\,,\ T=T_\infty\,,\ C=C_\infty \text{ at } y\to\infty \quad (6)$$

$\alpha=\frac{k}{(\rho c)_f}$ is the thermal diffusivity, $\tau=\frac{(\rho c)_p}{(\rho c)_f}$ is the ratio of nanoparticle heat capacity to base fluid heat capacity, Q_0 is the dimensional heat generation and absorption coefficient, δ_W is Wakif's coefficient. The concentration of nanoparticles at the surface C_w is higher than that of the surrounding fluid C_∞.

Using the Rosseland estimator, we may approximate the radiative heat flux:

$$q_r=-\frac{4\sigma^*}{3k^*}\frac{\partial T^4}{\partial y} \quad (7)$$

σ^* is the Stefan-Boltzmann constant, while $k^*$is the coefficient of mean absorption. Assuming little flow temperature variance, the equation for T^4 is linear function. Expanding T^4 in a Taylor series about T_∞ and eliminating the higher-order terms beyond the first degree in $(T-T_\infty)$ yields:

$$T^4=4T_\infty^3T-3T_\infty^4 \quad (8)$$

Consider the following nondimensional variables:

$$\eta=\sqrt{\frac{a}{\nu}}y\,,\ \psi(x,y)=\sqrt{a\nu}xf(\eta) \quad \theta(\eta)=\frac{T-T_\infty}{T_f-T_\infty}\,,\ \Phi(\eta)=\frac{C-C_\infty}{C_f-C_\infty} \quad (9)$$

Where $u = \frac{\partial \psi}{\partial y}$ and $= -\frac{\partial \psi}{\partial x}$, the continuity equation **(1)** is satisfied by the stream function $\psi(x, y)$. Equations **(2)**, **(4)**, and **(8)** are translated into the ODEs shown in Eq. **(9)**.

$$f''' - M^2 f' + (1 + \lambda M^2) f f'' - f'^2 - \lambda (f^2 f''' - 2 f f' f'') = 0 \quad \textbf{(10)}$$

$$(1 + N_r)\theta'' + P_r\left(f\theta' + \delta\theta + N_b \Phi'\theta' + N_t \theta'^2\right) = 0 \quad \textbf{(11)}$$

$$\Phi'' + L_e P_r f \Phi' + \frac{N_t}{N_b}\theta'' - \gamma L_e P_r \Phi = 0 \quad \textbf{(12)}$$

Here are the appropriate boundary conditions:

$$f(0) = 0\ ,\ f'(0) = 1\ ,\ \theta'(0) = -B_i\left(1 - \theta(0)\right)\ ,\ \Phi(0) = 1 \quad \textbf{(13)}$$
$$f'(\infty) = 0\ ,\ \theta(\infty) = 0\ ,\ \Phi(\infty) = 0$$

The prime represents differentiation with relation to η. The similarity function is denoted by$f$, while the Prandtl number is $P_r = \frac{\nu}{\alpha}$. $L_e = \frac{\alpha}{D_B}$ Represent the Lewis number, $B_i = \frac{h_f}{k}\sqrt{\frac{\nu}{\alpha}}$ is the Biot number, $\lambda = ak_0$ Is the elastic parameter, $\delta = \frac{Q_0}{a\rho c_p}$ is the heat generation/absorption parameter, $M = B_0\sqrt{\frac{\sigma}{a\rho_f}}$ is the magnetic parameter, $N_b = \frac{(\rho c)_p D_B (C_w - C_\infty)}{\delta_W (\rho c)_f \nu}$ is the Brownian motion parameter, $N_t = \frac{(\rho c)_p D_T (T_w - T_\infty)}{(\rho c)_f \nu T_\infty}$ is the thermophoresis parameter, $R = \frac{16\sigma^* {T_\infty}^3}{3kk^*}$ the radiation parameter,
The skin friction coefficientC_f, local Nusselt numberN_{u_x}, and local Sherwood number Sh_x are evaluated as follows:

$$C_f = \frac{\tau_w}{\rho {u_w}^2}\ , N_{u_x} = \frac{x q_w}{k\left(T_f - T_\infty\right)},\quad Sh_x = \frac{x h_m}{D_B (C_w - C_\infty)} \quad \textbf{(14)}$$

In this equation, τ_w represents shear stress, whereas q_w and h_m represent surface heat and mass flux.

$$\tau_w = \mu(1 + \lambda)\left(\frac{\partial u}{\partial y}\right)_{y=0},\quad q_w = -k\left(\frac{\partial T}{\partial y}\right)_{y=0}, h_m = D_B\left(\frac{\partial C}{\partial y}\right)_{y=0} \quad \textbf{(15)}$$

The similarity transformation converts the non-dimensional versions of skin friction, nusselt number, and sherwood number as follows:

$$Re_x^{\frac{1}{2}} C_f = (1 + \lambda) f''(0)\ , \quad \textbf{(16)}$$

$$\frac{N_{u_x}}{Re_x^{\frac{1}{2}}} = -\theta'(0)\ , \frac{Sh_x}{Re_x^{\frac{1}{2}}} = -\Phi'(0)$$

$Re_x = \frac{x U_w}{\nu}$ Represents the local Reynolds number.

3 The Runge-Kutta-Fehlberg Fourth-Order Method

The region $[0, \infty]$ has been replaced by the limited region $[0, \eta_\infty]$, where η_∞ is an acceptable real number. The solution must confirm the domain standard to solve the ODEs from **(10)** to **(12)**, as well as the initial and boundary conditions **(13)**. To solve **(10)** - **(12)**, we have seven first-order problems, each with seven variables.

$$\{f = y_1, f' = y_2, f'' = y_3, \theta = y_4, \theta' = y_4, \Phi = y_6, \Phi' = y_7\} \quad \textbf{(17)}$$

To create the most successful numerical strategy, we combine the shooting methodology with the Runge-Kutta-Fehlberg fourth-order method. Maple, a symbolic software, was used to obtain the numerical results. The model requires seven initial conditions, but only four are available: $\theta'(0)$, $f(0)$, $f'(0)$, and $\Phi(0)$. The remaining three, $f''(0)$, $\theta(0)$, and $\Phi'(0)$, were unavailable. To determine the necessary end boundary conditions, we use the shooting strategy, estimating the three beginning circumstances first. To obtain a result from the mathematical simulation, set the step length to $\Delta\eta = 0.001$ and the convergence condition to 10^{-8}. Figure 2 depicts the subsequent process.

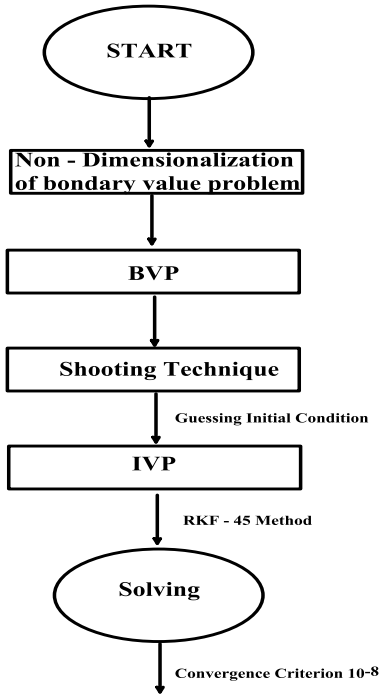

Fig. 2: chart of the computational process

4 The Variational Iteration Method

Consider the differential equation.

$$Lu + Nu = g(x) \quad \textbf{(18)}$$

L and N are linear and nonlinear operators, respectively, with $g(x)$ representing the source inhomogeneous term. The variational iteration method allows for the employment of a correction functional for equation **(17)** in the form.

$$U_{n+1}(x) = U_n(x) + \int_0^x \lambda(t)\left(LU_n(t) + N\widetilde{U}_n(t) - g(t)\right)dt \quad \textbf{(19)}$$

In this equation, λ represents a generic Lagrange's multiplier that can be ideally discovered using variational theory. $\widetilde{U}_n$ represents a restricted variation, with $\tau\widetilde{U}_n = 0$.The Lagrange multiplier λ plays a significant role in the procedure and can be either a constant or function. After determining λ, we apply an iteration method to calculate consecutive approximations of the answer $U(x)$: $U_{n+1}(x)$; $n > 0$. The zeroth approximation U_0 can be any selective function. However, the initial values $U(0)$, $U'(0)$, and $U''(0)$ are preferred for the selected zeroth approximation U_0, as will be demonstrated later. Thus, the solution is given by:

$$U(x) = \lim_{n\to\infty} U_n(x) \quad \textbf{(20)}$$

We officially derived the various forms of the Lagrange multipliers λ in [XX], therefore we will skip the details. We just provide an overview of the acquired results.

For first-order ODEs of the type:

$$U' + p(x)U = q(x)\,, U(0) = \alpha \quad \textbf{(21)}$$

The correction functional yields the iteration formula when λ is equal to -1.

$$U_{n+1}(x) = U_n(x) - \int_0^x \left(U'_n(t) + p(t)U_n(t) - q(t)\right)dt \quad \textbf{(22)}$$

For the second-order ODE.

$$U'' + aU'(x) + bU(x) = g(x)\,, U(0) = \alpha\,, U'(0) = \beta \quad \textbf{(23)}$$

$\lambda = t - x$, and the correction function yields the iteration formula.

$$U_{n+1}(x) = U_n(x) - \int_0^x (t - x)\left(U''_n(t) + aU'_n(t) + bU_n(t) - g(t)\right)dt \quad \textbf{(24)}$$

Furthermore, in the third-order ODE

$$U''' + aU'' + bU' + cU = g(x)\,, U(0) = \alpha\,, U'(0) = \beta\,, U''(0) = \gamma \quad \textbf{(25)}$$

We discovered that $\lambda = \frac{1}{2!}(t - x)^2$, and the iteration formula takes the form

$$U_{n+1}(x) = U_n(x) - \frac{1}{2!}\int_0^x (t - x)^2\left(U'''_n(t) + aU''_n(t) + bU'_n(t) + cU_n(t) - g(t)\right)dt \quad \textbf{(26)}$$

Typically, for the nth-order ODE

$$U^{(n)} + \mathrm{f}\left(U, U', U'', \ldots, U^{(n-1)}\right) = g(x), U(0) = \alpha_0\,, U'(0) = \alpha_1\,, U''(0) = \alpha_2\,, \ldots, U^{(n-1)}(0) = \alpha_{n-1} \quad \textbf{(27)}$$

We discovered that $\lambda = \frac{(-1)^n}{(n-1)!}(t - x)^{n-1}$, and the iteration formula takes the form

$$U_{n+1}(x) = U_n(x) - \frac{(-1)^n}{(n-1)!}\int_0^x (t - x)^{n-1}\left(U^{(n)} + \mathrm{f}\left(U, U', U'', \ldots, U^{(n-1)}\right) - g(t)\right)dt \quad \textbf{(28)}$$

The zeroth approximation $U_0(x)$ can be any selected function, although it is recommended to select it in the following form:

$$U_0(x) = U(0) + U'(0)x + \frac{1}{2!}U''(0)x^2 + \cdots + \frac{1}{n-1}U^{(n-1)}(0)x^{n-1} \quad \textbf{(29)}$$

Where n is the order of the ODE.

The three Figure 3, Figure 4 and Figure 5 represent the comparison of the results given by RK and VIM, therefore the results given by VIM are validated.

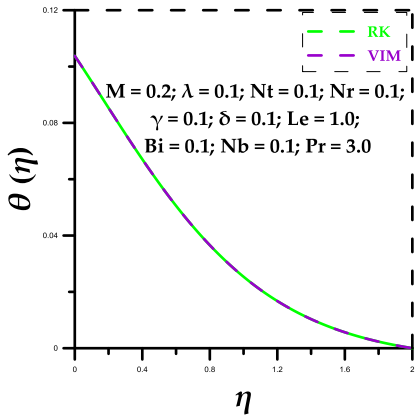

Fig. 3: Comparison between the results given by (RK) and (VIM) for $\theta(\eta)$

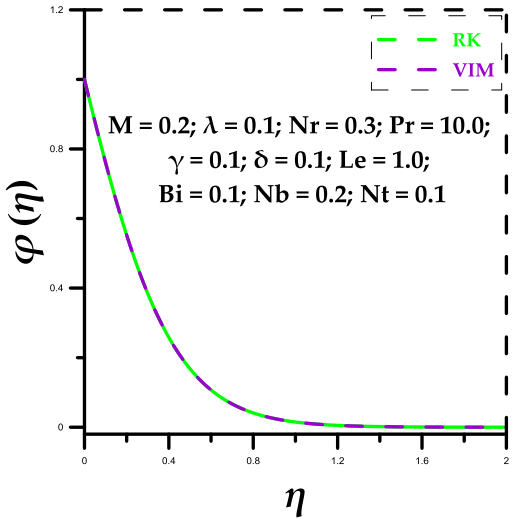

Fig. 4: Comparison between the results given by (RK) and (VIM) for $\Phi(\eta)$

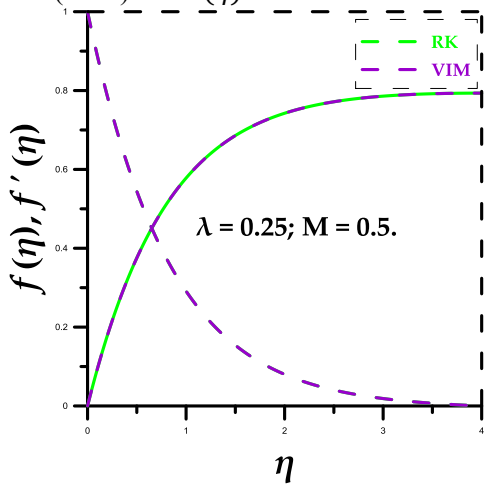

Fig. 5: Comparison between the results given by (RK) and (VIM) for $f(\eta)$ and $f'(\eta)$

5 Results and Discussions

Figure 6, Figure 7, Figure 8, Figure 9, Figure 10, Figure 11, Figure 12, Figure 13, Figure 14, Figure 15, Figure 16, Figure 17, Figure 18, Figure 19, Figure 20, Figure 21 show a model of a $2-D$ Maxwell fluid moving across a stretched sheet, including heat radiation and nanoparticles. Skin friction, Nusselt number, and the Sherwood number were calculated numerically, together with velocity, temperature, and concentration. This was accomplished through the use of numerous discrete nondimensional flow parameters. Figure 6 shows the temperature circulation of the thermal boundary layer with different thermophoresis parameter N_t values. When there is a temperature differential, a transport force called thermophoresis occurs. Increasing the amount of N_t increases the thickness of the boundary layer, which raises the surface temperature.

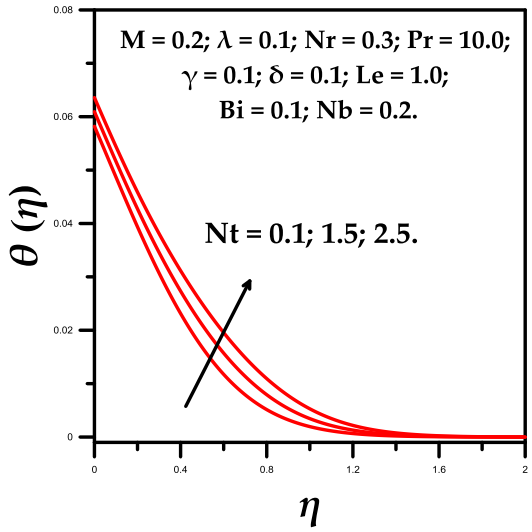

Fig. 6: Impact of N_t on temperature $\theta(\eta)$

Figure 7 shows the temperature dispersion of the thermal boundary layer with various Brownian motion N_b values. Brownian motion depicts how particles in a fluid move randomly and erratically due to repeated collisions with other molecules. This erratic mobility accelerates collisions between nanoparticles and molecules in the fluid. The molecules' kinetic energy converts to thermal energy, leading to an increase in temperature.

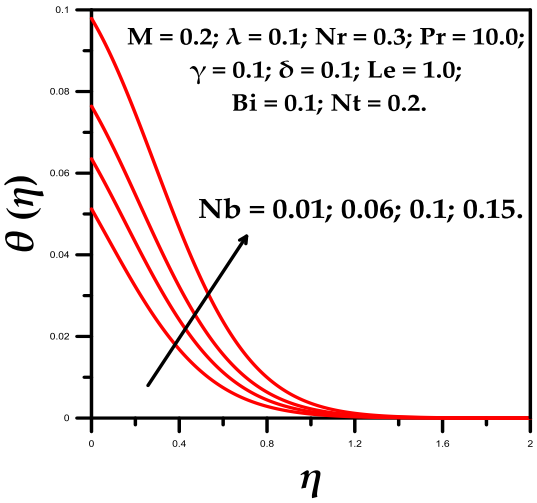

Fig. 7: Behavior of N_b on temperature $\theta(\eta)$

Figure 8 illustrates the temperature distribution of the thermal boundary layer with different Biot number approximations B_i. The Biot number refers to the ratio of the body's internal to external heat resistance. The ratio determines how much an external thermal gradient affects a body's internal temperature fluctuations over time. Problems with Biot numbers less than 1 are easily solved thermally due to homogenous temperature fields within the body. Higher Biot numbers indicate more complex challenges due to varying

temperature fields within the object. As the Biot number increases, the temperature near the boundary rises significantly. Convective heat transmission at the plate's surface leads to thicker thermal boundary layer.

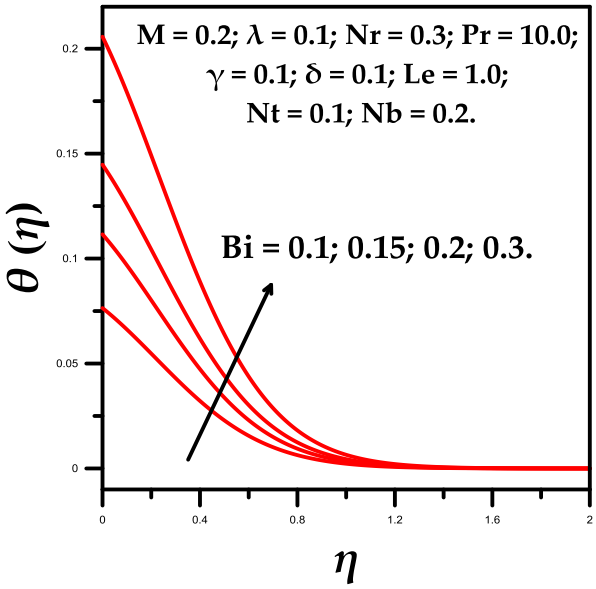

Fig. 8: Behavior of B_i on temperature $\theta(\eta)$

Figure 9 and Figure 10 depict temperature distributions for positive and negative scenarios based on altering chemical reaction parameter γ. In the boundary layer, damaging chemical reactions $\gamma > 0$ generate heat or thermal energy. This improves the thermal boundary layer. A generative chemical reaction ($\gamma < 0$) causes the fluid's temperature to decrease.

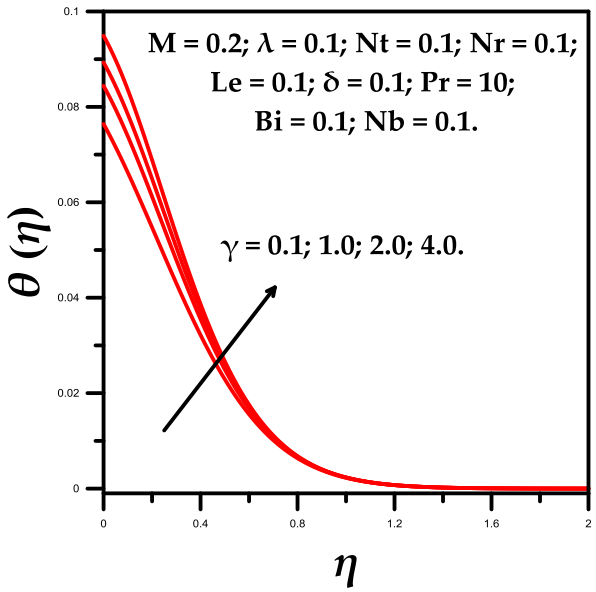

Fig. 9: Behavior of $+\gamma$ on temperature $\theta(\eta)$

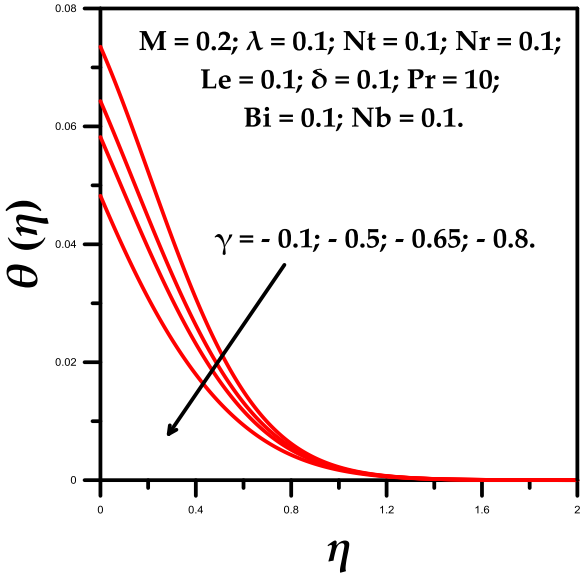

Fig. 10: Behavior of $-\gamma$ on temperature $\theta(\eta)$

Figure 11 and Figure 12 demonstrate how Le affects temperature and concentration. The Lewis number L_e represents the relationship between heat and mass diffusivity. Fluid flow is defined by the simultaneous transmission of heat and mass. The Lewis number compares the thicknesses of the thermal and concentration boundary layers. Increasing the Lewis number leads to increased thermal diffusivity and decreased Brownian diffusion. This means that the concentration decreases as the temperature increases.

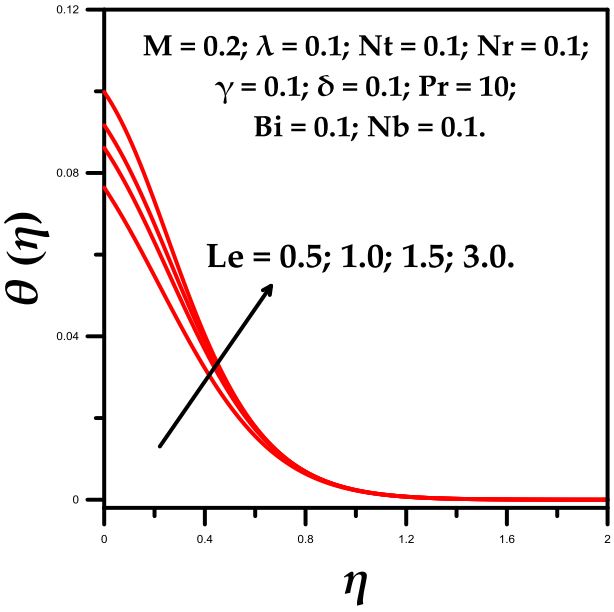

Fig. 11: Impact of L_e on temperature $\theta(\eta)$

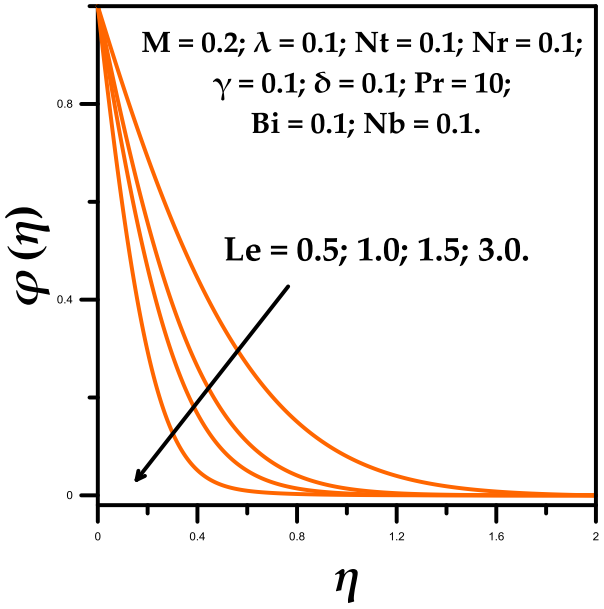

Fig. 12: Impact of L_e on concentration $\Phi(\eta)$

Figure 13 illustrates the temperature profiles for various Prandtl values. As the Prandtl number increases, the thermal boundary layer thins. Fluids with lower Prandtl numbers have better thermal conductivity and larger thermal boundary layer structures, allowing heat to escape the sheet faster than those with higher Prandtl numbers and thinner boundary layers. Changing the Prandtl number adjusts the cooling rate.

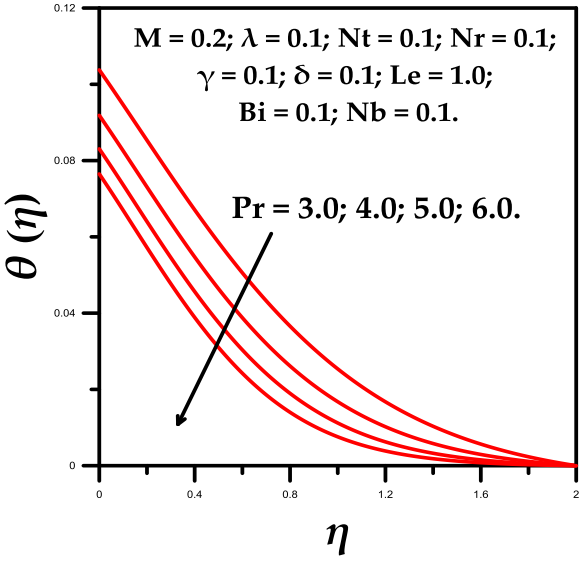

Fig. 13: Impact of P_r on temperature $\theta(\eta)$

Figure 14 displays the temperature curve for different radiation parameter N_r values. boosting the radiation parameter value increases temperature distribution by boosting surface heat transfer, resulting in hotter fluids.

Figure 15 illustrates how the concentration profiles change with the chemical reaction parameter γ. As the pace of a chemical reaction increases, the distribution of concentrations decreases. Rising γ predictions minimize the effects of buoyancy on concentration, resulting in a decline.

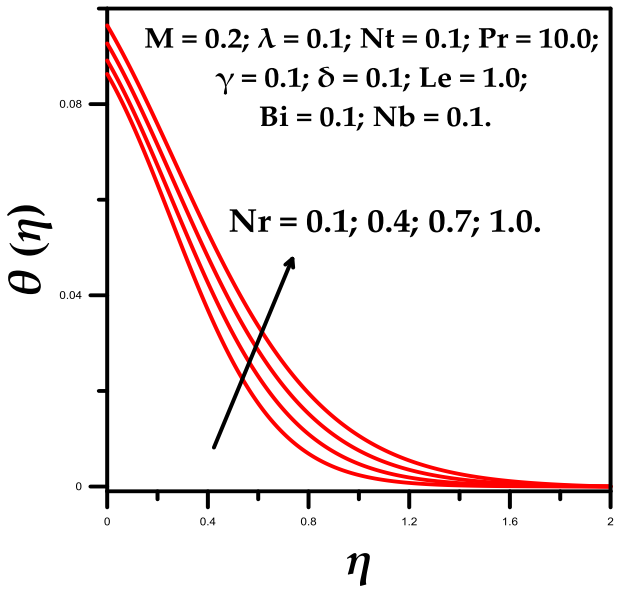

Fig. 14: Effect of N_r on temperature $\theta(\eta)$

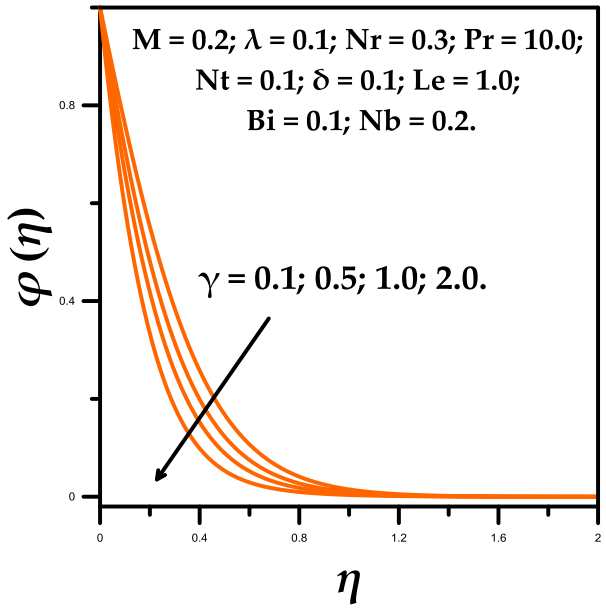

Fig. 15: Behavior of γ on concentration $\Phi(\eta)$

Figure 16 shows that increasing the amount of N_b at the surface leads to a drop in the fluid concentration. The Brownian motion warms the boundary layer, causing particles to move away from the fluid regime. However, further away from the surface, the opposite trend occurs.

Figure 17 illustrates the distribution of concentration in the thermal boundary layer for different thermophoresis parameter values N_t. Stronger thermophoresis results in a broader concentration boundary layer, leading to improved concentration.

Figure 18 and Figure 19 demonstrates that increasing the elastic parameter λ decreases the velocity distribution and thickness of the boundary layer. In terms of physics, relaxation time influences the elastic parameter. Longer relaxation times cause the fluid to travel slower.

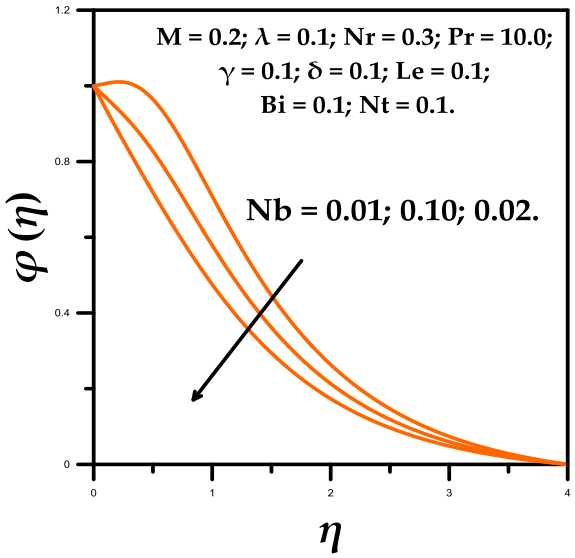

Fig. 16: Effect of N_b on concentration $\Phi(\eta)$

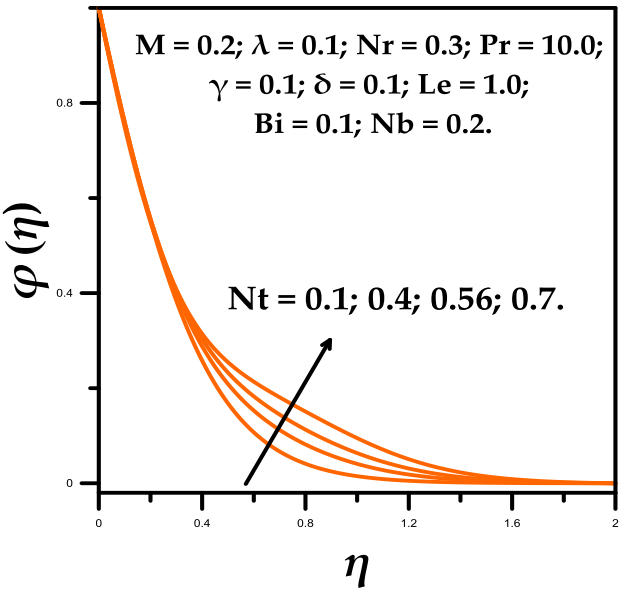

Fig. 17: Behavior of N_t on concentration $\Phi(\eta)$

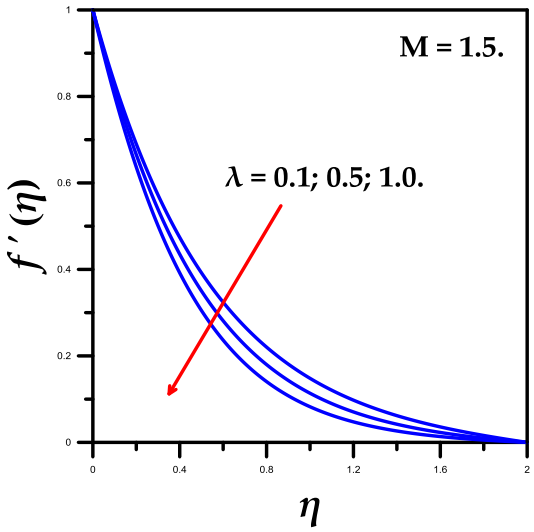

Fig. 18: Impact of λ on velocity $f'(\eta)$

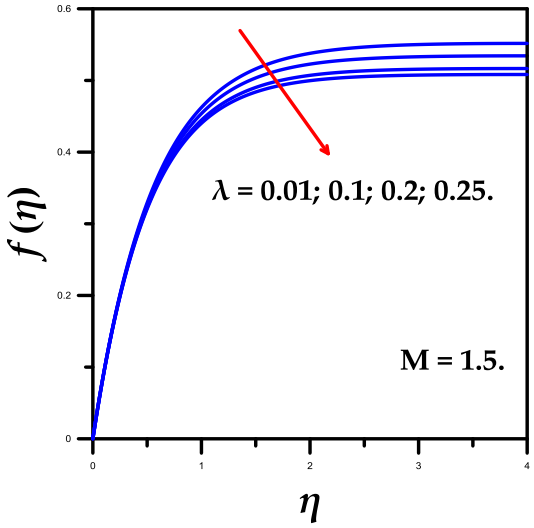

Fig. 19: Impact of λ on velocity $f(\eta)$

This reduces the velocity field and thickness of the boundary layer. As seen in Figure 15 and Figure 16, as the magnetic parameter M increases, the fluid velocity decreases. Persistent magnetic fields generate an opposing force known as drag force, which acts in the direction of fluid flow. Because of this obstruction, the momentum barrier layer may be thinner.

The velocity profile decreases when the magnetic field parameter increases as shown in both Figure 20 and Figure 21.

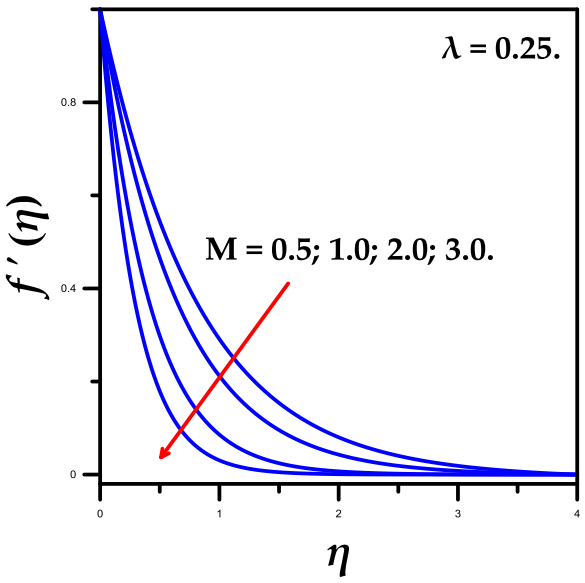

Fig. 20: Effect of M on velocity $f'(\eta)$

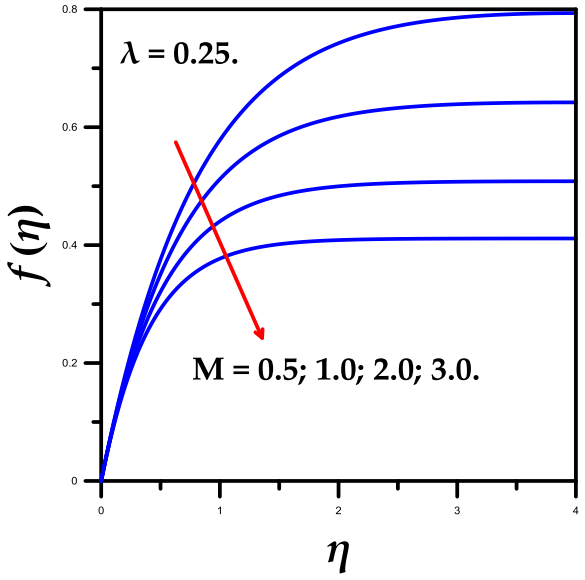

Fig. 21: Effect of M on velocity $f(\eta)$

6 Conclusions

We explored the heat and mass transport parameters of an incompressible steady $2-D$ Maxwell fluid as it flowed across a stretched sheet under thermal radiation and chemical interaction with Nanoparticles. The effect of embedded thermo-physical parameters on velocity, temperature, and concentration has been quantified. The variational iteration method aims to solve reduced ODEs by identifying equivalent solutions to existing ones. Compared to the RK-Fehlberg approach, the results are highly consistent.
The conclusions are as follows:

- As the level of M increases, velocities decrease.
- As P_r rises, temperature distributions flatten.
- As N_b approximations increase, Nusselt number approximations decrease.
- Sherwood predicts a rise in line with N_b estimations.
- Concentration profiles decrease as Le rises.
- Raising the estimations of N_r improves the temperature distribution.

References:

[1] T. Hayat, R. Sajjad, A. Alsaedi, T. Muhammad, R. Ellahi, On squeezed flow of couple stress nanofluid between two parallel plates, *Results Phys.*, 7 (2017) 553–561. https://doi.org/10.1016/j.rinp.2016.12.038.

[2] Y.-X. Li, M.H. Alshbool, Y.-P. Lv, I. Khan, M.R. Khan, A. Issakhov, Heat and mass transfer in MHD Williamson nanofluid flow over an exponentially porous stretching surface, *Case Stud. Therm. Eng.*, 26 (2021), 100975. https://doi.org/10.1016/j.csite.2021.100975.

[3] S. Ahmad, K. Ali, M. Rizwan, M. Ashraf, Heat and mass transfer attributes of copper–aluminum oxide hybrid nanoparticles flow through a porous medium, *Case Stud. Therm. Eng.*, 25 (2021), 100932. https://doi.org/10.1016/j.csite.2021.100932.

[4] M. Qureshi, Q. Rubbab, S. Irshad, S. Ahmad, M. Aqeel, Heat and mass transfer analysis of mhd nanofluid flow with radiative heat effects in the presence of spherical au-metallic nanoparticles, *Nanoscale Res. Lett.*, 11 (1) (2016) 1–11. https://doi.org/10.1186/s11671-016-1692-2.

[5] Amine El Harfouf, Rachid Herbazi, Sanaa Hayani Mounir, Hassane Mes-Adi, Abderrahim Wakif, "Heat and Mass Transfer Analysis of an unsteady Non-Newtonian Magnetohydrodynamic Fluid Flow (Semi-Analytical Solution)," *WSEAS Transactions on Heat and Mass Transfer*, vol. 18, pp. 182-194, 2023, https://doi.org/10.37394/232012.2023.18.15.

[6] Amine El Harfouf, Rachid Herbazi, Sanaa Hayani Mounir, Hassane Mes-Adi, Abderrahim Wakif, "Unsteady Compressed Williamson Fluid Flow Behavior under the Influence of a Fixed Magnetic Field (Numerical Study)," *WSEAS Transactions on Fluid Mechanics*, vol. 19, pp. 72-82, 2024, https://doi.org/10.37394/232013.2024.19.8.

[7] Amine El Harfouf, Rachid Herbazi, Sanaa Hayani Mounir, Hassane Mes-Adi, Abderrahim Wakif, "Non-Fourier Heat Flux Model for the Magnetohydrodynamic Casson Nanofluid Flow Past a Porous Stretching Sheet using the Akbari-Gangi Method," WSEAS Transactions on Fluid Mechanics, vol. 19, pp. 157-165, 2024, https://doi.org/10.37394/232013.2024.19.16.

[8] P. S. A. Reddy, A. Chamkha, Heat and mass transfer characteristics of MHD three-dimensional flow over a stretching sheet filled with water-based alumina nanofluid, *Int. J. Numer. Methods Heat Fluid Flow*, (2018). https://doi.org/10.1108/HFF-02-2017-0061.

[9] T. Hayat, R.S. Saif, R. Ellahi, T. Muhammad, B. Ahmad, Numerical study of boundary-layer flow due to a nonlinear curved stretching sheet with convective heat and mass conditions, *Results Phys.*, 7 (2017) 2601–2606. https://doi.org/10.1016/j.rinp.2017.07.023.

[10] M. Ferdows, M.J. Uddin, A. Afify, Scaling group transformation for MHD boundary layer free convective heat and mass transfer flow past a convectively heated nonlinear radiating stretching sheet, *Int. J. Heat Mass Tran.*, 56 (1–2) (2013) 181–187. https://doi.org/10.1016/j.ijheatmasstransfer.2012.09.020.

[11] Amine El Harfouf, Rachid Herbazi, Walid Abouloifa, Sanaa Hayani Mounir, Hassane Mes-Adi, Abderrahim Wakif, Mohamed Mejdal, Mohamed Nfaoui, "Numerical Examination of a Squeezing Casson Hybrid Nanofluid Flow Considering Thermophoretic and Internal Heating Mechanisms," *WSEAS Transactions on Heat and Mass Transfer*, vol. 19, pp. 41-51, 2024, https://doi.org/10.37394/232012.2024.19.5.

[12] S. Nadeem, R.U. Haq, Z. Khan, Numerical study of MHD boundary layer flow of a Maxwell fluid past a stretching sheet in the presence of nanoparticles, *J. Taiwan Inst. Chem. Eng.*, 45 (1) (2014) 121–126. https://doi.org/10.1016/j.jtice.2013.04.006.

[13] M. Mustafa, J.A. Khan, T. Hayat, A. Alsaedi, Simulations for Maxwell fluid flow past a convectively heated exponentially stretching sheet with nanoparticles, *AIP Adv.*, 5 (3) (2015), 037133. https://doi.org/10.1063/1.4916364.

[14] G. Ramesh, B. Gireesha, Influence of heat source/sink on a Maxwell fluid over a stretching surface with convective boundary condition in the presence of nanoparticles, *Ain Shams Eng. J.*, 5 (3) (2014) 991–998. https://doi.org/10.1016/j.asej.2014.04.003.

[15] Mohamad Isa, S., Mahat, R., Katbar, N. M., Goud, B. S., Ullah, I., Jamshed, W. Hussain, S. M. (2024). Thermal radiative and Hall current effects on magneto-natural convective flow of dusty fluid: Numerical Runge–Kutta–Fehlberg technique. *Numerical Heat Transfer, Part B: Fundamentals,* 1–23. https://doi.org/10.1080/10407790.2024.2318452.

[16] Y. Dharmendar Reddy, F. Mebarek-Oudina, B.S. Goud, A.I. Ismail, Radiation, velocity and thermal slips effect toward MHD boundary layer flow through heat and mass transport of Williamson nanofluid with porous medium, *Arabian J. Sci. Eng.*, 47 (12) (2022) 16355–16369, https://doi.org/10.1007/s13369-022-06825-2.

[17] G. Ramesh, B. Gireesha, T. Hayat, A. Alsaedi, MHD flow of Maxwell fluid over a stretching sheet in the presence of nanoparticles, thermal radiation and chemical reaction: a numerical study, *J. Nanofluids*, 4 (1) (2015) 100–106. https://doi.org/10.1166/jon.2015.1133.

[18] P. S. Narayana, D.H. Babu, Numerical study of MHD heat and mass transfer of a Jeffrey fluid over a stretching sheet with chemical reaction and thermal radiation, *J. Taiwan Inst. Chem. Eng.*, 59 (2016) 18–25. https://doi.org/10.1016/j.jtice.2015.07.014.

[19] S. Mukhopadhyay, Slip effects on MHD boundary layer flow over an exponentially stretching sheet with suction/blowing and thermal radiation, *Ain Shams Eng. J.*, 4 (3) (2013) 485–491. https://doi.org/10.1016/j.asej.2012.10.007.

[20] He JH. Variational iteration method—a kind of non-linear analytical technique: some examples. *Int J NonLin Mech.*, 1999; 34: 699–708. https://doi.org/10.1016/S0020-7462(98)00048-1.

[21] He JH. Some asymptotic methods for strongly nonlinear equations. *Int J. Mod. Phys. B.*, 2006; 20: 1141–1199. https://doi.org/10.1142/S0217979206033796.

[22] He JH. Variational iteration method—some recent results and new interpretations. *J. Comput. Appl. Math.*, 2007; 207: 3–17. https://doi.org/10.1016/j.cam.2006.07.009.

[23] Biazar J, Gholamin P, Hosseini K. Variational iteration method for solving Fokker–Planck

equation. *J. Franklin I,* 2010; 347: 1137–1147. https://doi.org/10.1016/j.jfranklin.2010.04.007.

[24] Jafari H. A comparison between the variational iteration method and the successive approximations method. *Appl. Math. Lett. 2014;* 32: 1–5. https://doi.org/10.1016/j.aml.2014.02.004.

[25] Odibat Z, Momani S. The variational iteration method: an efficient scheme for handling fractional partial differential equations in fluid mechanics. *Comput. Math. Appl.*, 2009; 58: 2199–2208. https://doi.org/10.1016/j.camwa.2009.03.009.

[26] A. Wakif, M. Zaydan, A.S. Alshomrani, T. Muhammad, and R. Sehaqui, "New insights into the dynamics of alumina-(60% ethylene glycol+40% water) over an isothermal stretching sheet using a renovated Buongiorno's approach: A numerical GDQLLM analysis," Int. Commun. *Heat Mass Transf.*, 133, 105937 (2022). https://doi.org/10.1016/j.icheatmasstransfer.2022.105937.

[27] A. Wakif, M. Zaydan, and R. Sehaqui, "Further insights into steady three-dimensional MHD Sakiadis flows of radiating-reacting viscoelastic nanofluids via Wakif's-Buongiorno and Maxwell's models," *J. Umm Al-Qura Univ. Appl. Sci.,* 1-13 (2024). https://doi.org/10.1007/s43994-024-00141-1.

[28] A. El Harfouf, A. Wakif, and S. Hayani Mounir, "New insights into MHD squeezing flows of reacting-radiating Maxwell nanofluids via Wakif's-Buongiorno point of view," *J. Umm Al-Qura Univ. Appl. Sci.,* 1-15 (2024). https://doi.org/10.1007/s43994-024-00139-9.

[29] M. Alghamdi, A. Wakif, and T. Muhammad, "Efficient passive GDQLL scrutinization of an advanced steady EMHD mixed convective nanofluid flow problem via Wakif-Buongiorno approach and generalized transport laws," *Int. J. Mod. Phys. B,* 2450418 (2024). https://doi.org/10.1142/S0217979224504186.

[30] A. Wakif, M. Zaydan, and R. Sehaqui, " Aspects of EMHD Boundary Layer Flows of Alumina-Water Nanofluidic Mixtures in a Porous Medium.," *J. Umm Al-Qura Univ. Appl. Sci.,* 1-9 (2024). https://doi.org/10.1007/s43994-024-00174-6.

Contribution of Individual Authors to the Creation of a Scientific Article (Ghostwriting Policy)

A. EL Harfouf: Conceptualization, Formal analysis, Investigation, Methodology, Project administration, Resources, Validation, Writing – original draft, Data curation, Software, Visualization. Conceptualization, Formal analysis, Investigation, Methodology, Project administration, Resources, Validation, Writing – review & editing. Conceptualization, Investigation, Writing – review & editing. Conceptualization, Formal analysis, Investigation, Methodology, Project administration, Resources, Validation, Writing – review & editing. **A. Wakif:** Conceptualization, Investigation, Project administration, Supervision, Writing – review & editing. Conceptualization, Formal analysis, Investigation, Methodology, Project administration, Resources, Validation, Writing – review & editing. Conceptualization, Investigation, Project administration, Writing – review & editing. **S. Hayani Mounir:** Conceptualization, Investigation, Project administration, Supervision, Writing – review & editing.

Sources of Funding for Research Presented in a Scientific Article or Scientific Article Itself

No funding was received for conducting this study.

Conflict of Interest

The authors have no conflicts of interest to declare.